# Hygro-thermal vibrations and buckling of laminated nanoplates via nonlocal strain gradient theory



*Published Version:*
Tocci Monaco G., Fantuzzi N., Fabbrocino F., Luciano R. (2021). Hygro-thermal vibrations and buckling of laminated nanoplates via nonlocal strain gradient theory. COMPOSITE STRUCTURES, 262, 1-10 [10.1016/j.compstruct.2020.113337].

*Availability:*
This version is available at: https://hdl.handle.net/11585/809903 since: 2024-09-19

*Published:*
DOI: http://doi.org/10.1016/j.compstruct.2020.113337

# Hygro-Thermal Vibrations and Buckling of laminated nanoplates via Nonlocal Strain Gradient Theory

Giovanni Tocci Monaco[1,2], Nicholas Fantuzzi[1,*], Francesco Fabbrocino[3], Raimondo Luciano[2]

**Abstract**

Vibrations and buckling of thin laminiated composite nano plates in hygrothermal environment are investigated using second-order strain gradient theory. Hamilton's principle is used in order to carry out motion equations. To obtain analytical solution Navier displacement field has been considered for both cross- and angle-ply laminates. Numerical solutions are provided and discussed in terms of plate aspect ratio and non local ratio for a large number of laminates. Whenever possible a comparison with classical analytical solutions is reported for buckling loads and fundamental frequencies. This work shows a large variety of angle-ply cases which are not common in the published literature. Moreover, critical temperatures for cross- and angle-ply laminates are shown for buckling and free vibration analyses.

*Keywords:* Kirchhoff plate's theory, Non-local theory, Strain gradient theory, Hygrothermal load, Buckling, Free vibration, Composite nanoplates, Cross- and Angle-ply laminates

## 1. Introduction

In the last decades MEMS (Micro-Electro-Mechanical-System) and NEMS (Nano-Electro-Mechanical-System) have become topics of great interest because of their large number of applications in many industrial fields [1, 2, 3, 4]. These kind of structures, such as nanoplates, nanorods, nanobeams, can be

*Corresponding email: nicholas.fantuzzi@unibo.it
[1]DICAM Department University of Bologna, Italy
[2]Engineering Department, Parthenope University, Italy
[3]Department of Engineering, Telematic University Pegaso, Italy

used in medicine [5], electronics [6], aerospace [7] and even in civil construction [8]. To properly describe the behaviour of nanostructures it is necessary to use theories that take into account the nano size effect, like long range atomic interaction [9, 10]. Effects at the nano scale have been experimentally measured in [11, 12]. Non-local theories have been widely used for the study of nanostructures since Eringen developed his theory of non-local elasticity [13]. These theories consider the nano scale effects thanks to the introduction of one or more length scale parameters in addition to well know linear elastic Lamé parameters [14, 15, 16, 17]. The classification of nonlocal theories is generally presented as: strain gradient [18, 19, 20, 21], stress gradient [22], modified strain gradient [23, 24, 25], couple stress [26], modified couple stress [27, 28], integral type [29, 30] and micropolar [31, 32, 33]. In [34] strain and stress gradient non local theory is used to study dynamic and buckling problems of elastic nanobeams. Nanoplates subjected to hygrothermal loads were also investigated in the works [35, 36, 37, 38], using different non-local theories. In [39, 40] the influence of the non-local parameter on the critical load is studied and the solution for the problem of buckling of ccomposite nanoplates is provided. In [41] different non-local theories were employed to model the vibrational behavior of plates. Civalek et al. [42] presented numerical studies for dimensionless natural frequencies of different truss and frame models, investigating the influences of the nonlocal parameter. In [43], thermally induced dynamic behaviors of functionally graded flexoelectric nanobeams (FGFNs) are analyzed using semplified strain gradient nonlocal theory. The effect of thermal, hygrometric and piezoelectric stress on composite plates and shells has been investigated by [44, 45, 46, 47].

The focus of this paper is the study of buckling and free vibrations of laminated composite nano plates in hygrothermal environment. In particular, for the buckling analysis it will look for the temperature value and the combination of temperature and humidity that leads to the instability of the plate, while for the dynamic case it will investigate the influence that the thermal load has on the natural vibration frequencies. This paper is structured as described below. After the introduction section, the theoretical background for laminated thin plates in hygrothermal environment is developed introducing also the non-linear terms of von Karman that allow to perform the linear analysis of buckling. Using second order strain gradient theory non local effect are take into account. The analytical solution is obtained using Navier developments in double trigonometric series. Then, in order to validate the calculation code, implemented in MATLAB, various comparisons with the

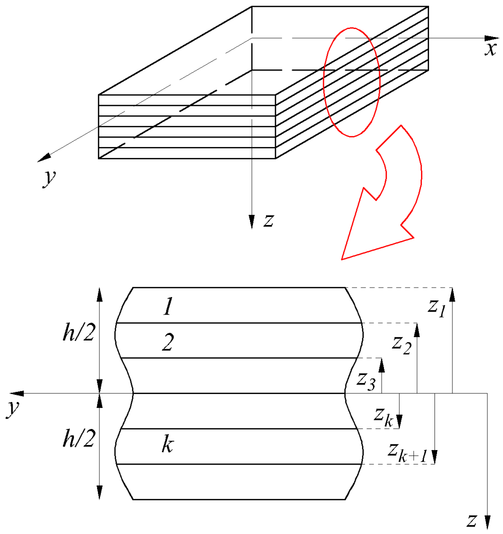


Figure 1: Laminate general layout.

literature are reported [48, 49, 50, 51]. After the comparisons, the results for buckling and free vibration obtained for different lamination schemes and different types of load are provided. Finally, a conclusion section is reported at the end of this paper.

## 2. Theoretical background

Consider a laminated thin nanoplate, modeled with the Kirchhoff plate assumptions modified to take into account the non linear terms of von Karman, subjected to hygrothermal stresses. The plate is composed of $k$ orthotropic layers oriented at angles $\theta^{(1)}$, $\theta^{(2)}$, ..., $\theta^{(k)}$. The thickness of the $k$-th oriented layer, along the $z$ axis, is defined as $h_k = z_{k+1} - z_k$. Introduced the reference system as in figure 1, we can define the displacement field of a generic point of the solid by means of the triad of displacement components $U$, $V$, $W$, which are functions of the coordinates $(x, y, z)$.

$$
\begin{aligned}
U(x, y, z, t) &= u(x, y, t) - z\frac{\partial w}{\partial x} \\
V(x, y, z, t) &= v(x, y, t) - z\frac{\partial w}{\partial y} \\
W(x, y, z, t) &= w(x, y, t)
\end{aligned}
\tag{1}
$$

where $u$,$v$ and $w$ are the displacements along the $x$, $y$ and $z$ axis of the point on the middle surface and $\partial w/\partial x$ and $\partial w/\partial y$ are the corresponding rotations. The plate strains are defined as:

$$\boldsymbol{\varepsilon} = \boldsymbol{\varepsilon}^{(0)} + z\boldsymbol{\varepsilon}^{(1)} \tag{2}$$

where

$$\boldsymbol{\varepsilon}^{(0)} = \begin{Bmatrix} \varepsilon_{xx}^{(0)} \\ \varepsilon_{yy}^{(0)} \\ \gamma_{xy}^{(0)} \end{Bmatrix} = \begin{Bmatrix} \frac{\partial u}{\partial x} + \frac{1}{2}\left(\frac{\partial w}{\partial x}\right)^2 \\ \frac{\partial v}{\partial y} + \frac{1}{2}\left(\frac{\partial w}{\partial y}\right)^2 \\ \frac{\partial u}{\partial y} + \frac{\partial v}{\partial x} + \frac{\partial w}{\partial x}\frac{\partial w}{\partial y} \end{Bmatrix}, \quad \boldsymbol{\varepsilon}^{(1)} = \begin{Bmatrix} \varepsilon_{xx}^{(1)} \\ \varepsilon_{yy}^{(1)} \\ \gamma_{xy}^{(1)} \end{Bmatrix} = \begin{Bmatrix} -\frac{\partial^2 w}{\partial x^2} \\ -\frac{\partial^2 w}{\partial y^2} \\ -2\frac{\partial^2 w}{\partial x \partial y} \end{Bmatrix} \tag{3}$$

In order to take into account non local effects, the second order strain gradient theory is introduced as follows

$$\begin{aligned} \begin{Bmatrix} \sigma_{xx} \\ \sigma_{yy} \\ \sigma_{xy} \end{Bmatrix}^{(k)} &= \left(1 - \ell^2 \nabla^2\right) \begin{bmatrix} \bar{Q}_{11} & \bar{Q}_{12} & \bar{Q}_{16} \\ \bar{Q}_{12} & \bar{Q}_{22} & \bar{Q}_{26} \\ \bar{Q}_{16} & \bar{Q}_{26} & \bar{Q}_{66} \end{bmatrix}^{(k)} \begin{Bmatrix} \varepsilon_{xx} \\ \varepsilon_{yy} \\ \gamma_{xy} \end{Bmatrix} \\ &- \begin{bmatrix} \bar{Q}_{11} & \bar{Q}_{12} & \bar{Q}_{16} \\ \bar{Q}_{12} & \bar{Q}_{22} & \bar{Q}_{26} \\ \bar{Q}_{16} & \bar{Q}_{26} & \bar{Q}_{66} \end{bmatrix}^{(k)} \begin{Bmatrix} \alpha_{xx}\Delta T + \beta_{xx}\Delta C \\ \alpha_{yy}\Delta T + \beta_{yy}\Delta C \\ 2\alpha_{xy}\Delta T + 2\beta_{xy}\Delta C \end{Bmatrix}^{(k)} \end{aligned} \tag{4}$$

where the subscript $^{(k)}$ indicates the $k$-th orthotropic lamina, $\ell$ is the nonlocal parameter and the operator $\nabla^2 = \partial^2/\partial x^2 + \partial^2/\partial y^2$.

A linear variation of hygrothermal loads along the thickness is assumed:

$$\begin{aligned} \Delta T &= T_0 + zT_1/h \\ \Delta C &= C_0 + zC_1/h \end{aligned} \tag{5}$$

It is underlined that the $\bar{Q}_{ij}^{(k)}$ represent the engineering constants oriented towards the reference system of the problem [48]. The hygrothermal properties of each ply have to be oriented also:

$$\begin{aligned} \boldsymbol{\alpha}^{(k)} &= \begin{Bmatrix} \alpha_{xx} \\ \alpha_{yy} \\ 2\alpha_{xy} \end{Bmatrix}^{(k)} = \begin{Bmatrix} \alpha_1^{(k)} \cos^2\theta^{(k)} + \alpha_2^{(k)} \sin^2\theta^{(k)} \\ \alpha_1^{(k)} \sin^2\theta^{(k)} + \alpha_2^{(k)} \cos^2\theta^{(k)} \\ 2\left(\alpha_1^{(k)} - \alpha_2^{(k)}\right) \sin\theta^{(k)} \cos\theta^{(k)} \end{Bmatrix} \\ \boldsymbol{\beta}^{(k)} &= \begin{Bmatrix} \beta_{xx} \\ \beta_{yy} \\ 2\beta_{xy} \end{Bmatrix}^{(k)} = \begin{Bmatrix} \beta_1^{(k)} \cos^2\theta^{(k)} + \beta_2^{(k)} \sin^2\theta^{(k)} \\ \beta_1^{(k)} \sin^2\theta^{(k)} + \beta_2^{(k)} \cos^2\theta^{(k)} \\ 2\left(\beta_1^{(k)} - \beta_2^{(k)}\right) \sin\theta^{(k)} \cos\theta^{(k)} \end{Bmatrix} \end{aligned} \tag{6}$$

By integrating the stresses along the thickness we obtain:

$$\begin{aligned}
\mathbf{N} = \begin{Bmatrix} N_{xx} \\ N_{yy} \\ N_{xy} \end{Bmatrix} = \sum_{k=1}^{N_L} \int_{z_k}^{z_{k+1}} \begin{Bmatrix} \sigma_{xx} \\ \sigma_{yy} \\ \sigma_{xy} \end{Bmatrix}^{(k)} dz \\
\mathbf{M} = \begin{Bmatrix} M_{xx} \\ M_{yy} \\ M_{xy} \end{Bmatrix} = \sum_{k=1}^{N_L} \int_{z_k}^{z_{k+1}} \begin{Bmatrix} \sigma_{xx} \\ \sigma_{yy} \\ \sigma_{xy} \end{Bmatrix}^{(k)} z\ dz
\end{aligned} \tag{7}$$

Such definition of stress resultants allows to define $\mathbf{A}$,$\mathbf{D}$ and $\mathbf{B}$ matrices, called *membrane stiffness matrix, bending stiffness matrix* and *bending-membrane coupling stiffness matrix* [48], and vectors $\mathbf{A}^\alpha$, $\mathbf{A}^\beta$,$\mathbf{B}^\alpha$, $\mathbf{B}^\beta$, $\mathbf{D}^\alpha$ and $\mathbf{D}^\beta$ containing the hygrothermal properties of the laminate

$$\begin{aligned}
\mathbf{A}^\alpha &= \sum_{k=1}^{N_L} \int_{z_k}^{z_{k+1}} \bar{\mathbf{Q}}^{(k)} \boldsymbol{\alpha}^{(k)} dz = \sum_{k=1}^{N_L} \bar{\mathbf{Q}}^{(k)} \boldsymbol{\alpha}^{(k)} \left(z_{k+1} - z_k\right) \\
\mathbf{B}^\alpha &= \sum_{k=1}^{N_L} \int_{z_k}^{z_{k+1}} \bar{\mathbf{Q}}^{(k)} \boldsymbol{\alpha}^{(k)} z\ dz = \frac{1}{2} \sum_{k=1}^{N_L} \bar{\mathbf{Q}}^{(k)} \boldsymbol{\alpha}^{(k)} \left(z_{k+1}^2 - z_k^2\right) \\
\mathbf{D}^\alpha &= \sum_{k=1}^{N_L} \int_{z_k}^{z_{k+1}} \bar{\mathbf{Q}}^{(k)} \boldsymbol{\alpha}^{(k)} z^2\ dz = \frac{1}{3} \sum_{k=1}^{N_L} \bar{\mathbf{Q}}^{(k)} \boldsymbol{\alpha}^{(k)} \left(z_{k+1}^3 - z_k^3\right)
\end{aligned} \tag{8}$$

$$\begin{aligned}
\mathbf{A}^\beta &= \sum_{k=1}^{N_L} \int_{z_k}^{z_{k+1}} \bar{\mathbf{Q}}^{(k)} \boldsymbol{\beta}^{(k)} dz = \sum_{k=1}^{N_L} \bar{\mathbf{Q}}^{(k)} \boldsymbol{\beta}^{(k)} \left(z_{k+1} - z_k\right) \\
\mathbf{B}^\beta &= \sum_{k=1}^{N_L} \int_{z_k}^{z_{k+1}} \bar{\mathbf{Q}}^{(k)} \boldsymbol{\beta}^{(k)} z\ dz = \frac{1}{2} \sum_{k=1}^{N_L} \bar{\mathbf{Q}}^{(k)} \boldsymbol{\beta}^{(k)} \left(z_{k+1}^2 - z_k^2\right) \\
\mathbf{D}^\beta &= \sum_{k=1}^{N_L} \int_{z_k}^{z_{k+1}} \bar{\mathbf{Q}}^{(k)} \boldsymbol{\beta}^{(k)} z^2 dz = \frac{1}{3} \sum_{k=1}^{N_L} \bar{\mathbf{Q}}^{(k)} \boldsymbol{\beta}^{(k)} \left(z_{k+1}^3 - z_k^3\right)
\end{aligned} \tag{9}$$

the stress characteristics take the following form:

$$\begin{Bmatrix} N_{xx} \\ N_{yy} \\ N_{xy} \end{Bmatrix} = \left(1-\ell^2\nabla^2\right) \left( \begin{bmatrix} A_{11} & A_{12} & A_{16} \\ A_{12} & A_{22} & A_{26} \\ A_{16} & A_{26} & A_{66} \end{bmatrix} \begin{Bmatrix} \varepsilon_{xx}^{(0)} \\ \varepsilon_{yy}^{(0)} \\ \gamma_{xy}^{(0)} \end{Bmatrix} + \begin{bmatrix} B_{11} & B_{12} & B_{16} \\ B_{12} & B_{22} & B_{26} \\ B_{16} & B_{26} & B_{66} \end{bmatrix} \begin{Bmatrix} \varepsilon_{xx}^{(1)} \\ \varepsilon_{yy}^{(1)} \\ \gamma_{xy}^{(1)} \end{Bmatrix} \right)$$
$$- \begin{Bmatrix} A_1^\alpha \\ A_2^\alpha \\ A_6^\alpha \end{Bmatrix} T_0 - \begin{Bmatrix} B_1^\alpha \\ B_2^\alpha \\ B_6^\alpha \end{Bmatrix} \frac{1}{h} T_1 - \begin{Bmatrix} A_1^\beta \\ A_2^\beta \\ A_6^\beta \end{Bmatrix} C_0 - \begin{Bmatrix} B_1^\beta \\ B_2^\beta \\ B_6^\beta \end{Bmatrix} \frac{1}{h} C_1 \tag{10}$$

$$\begin{Bmatrix} M_{xx} \\ M_{yy} \\ M_{xy} \end{Bmatrix} = \left(1-\ell^2\nabla^2\right) \left( \begin{bmatrix} B_{11} & B_{12} & B_{16} \\ B_{12} & B_{22} & B_{26} \\ B_{16} & B_{26} & B_{66} \end{bmatrix} \begin{Bmatrix} \varepsilon_{xx}^{(0)} \\ \varepsilon_{yy}^{(0)} \\ \gamma_{xy}^{(0)} \end{Bmatrix} + \begin{bmatrix} D_{11} & D_{12} & D_{16} \\ D_{12} & D_{22} & D_{26} \\ D_{16} & D_{26} & D_{66} \end{bmatrix} \begin{Bmatrix} \varepsilon_{xx}^{(1)} \\ \varepsilon_{yy}^{(1)} \\ \gamma_{xy}^{(1)} \end{Bmatrix} \right)$$
$$- \begin{Bmatrix} B_1^\alpha \\ B_2^\alpha \\ B_6^\alpha \end{Bmatrix} T_0 - \begin{Bmatrix} D_1^\alpha \\ D_2^\alpha \\ D_6^\alpha \end{Bmatrix} \frac{1}{h} T_1 - \begin{Bmatrix} B_1^\beta \\ B_2^\beta \\ B_6^\beta \end{Bmatrix} C_0 - \begin{Bmatrix} D_1^\beta \\ D_2^\beta \\ D_6^\beta \end{Bmatrix} \frac{1}{h} C_1 \tag{11}$$

In order to carry out the equations of motion the Hamilton's principle is employed

$$\int_0^T \left(\delta U + \delta V - \delta K\right)\, dt = 0 \tag{12}$$

where $\delta U$ is the virtual strain energy, $\delta V$ is the virtual work done by the applied forces and $\delta K$ is the virtual kinetic energy. Developing the terms in equation (12) the Hamilton's principle takes the following form:

$$\int_0^T \left[ \int_{\mathcal{A}} \left[ \begin{Bmatrix} \delta u_{,x} \\ \delta u_{,y} \\ \delta v_{,x} \\ \delta v_{,y} \\ \delta w_{,xx} \\ \delta w_{,yy} \\ \delta w_{,xy} \end{Bmatrix}^\top \begin{bmatrix} \mathcal{T}_{11} & \mathcal{T}_{12} & \mathcal{T}_{13} \\ \mathcal{T}_{21} & \mathcal{T}_{22} & \mathcal{T}_{23} \\ \mathcal{T}_{31} & \mathcal{T}_{32} & \mathcal{T}_{33} \\ \mathcal{T}_{41} & \mathcal{T}_{42} & \mathcal{T}_{43} \\ \mathcal{T}_{51} & \mathcal{T}_{52} & \mathcal{T}_{53} \\ \mathcal{T}_{61} & \mathcal{T}_{62} & \mathcal{T}_{63} \\ \mathcal{T}_{71} & \mathcal{T}_{72} & \mathcal{T}_{73} \end{bmatrix} \begin{Bmatrix} u \\ v \\ w \end{Bmatrix} - \begin{Bmatrix} \delta w_{,x} & \delta w_{,y} \end{Bmatrix} \begin{bmatrix} \hat{N}_{xx} & \hat{N}_{xy} \\ \hat{N}_{xy} & \hat{N}_{yy} \end{bmatrix} \begin{Bmatrix} w_{,x} \\ w_{,y} \end{Bmatrix} \right.\right.$$
$$\left.\left. \begin{Bmatrix} \delta \ddot{u} \\ \delta \ddot{v} \\ \delta \ddot{w} \\ \delta \ddot{w}_{,x} \\ \delta \ddot{w}_{,y} \end{Bmatrix}^\top \begin{bmatrix} I_0 & 0 & 0 & -I_1 & 0 \\ 0 & I_0 & 0 & 0 & -I_1 \\ 0 & 0 & I_0 & 0 & 0 \\ -I_1 & 0 & 0 & I_2 & 0 \\ 0 & -I_1 & 0 & 0 & I_2 \end{bmatrix} \begin{Bmatrix} \delta u \\ \delta v \\ \delta w \\ \delta w_{,x} \\ \delta w_{,y} \end{Bmatrix} \right] dxdy \right] dt$$
$$+ \text{boundary integral terms} = 0 \tag{13}$$

where the variational form of the displacement field is identified by $\delta$, while its corresponding derivatives in time by the dots, the terms $\mathcal{T}_{ij}$ are shown in [52], $\hat{N}_{xx}$, $\hat{N}_{yy}$ and $\hat{N}_{xy}$ (defined in eq. (10)) identify the axial and shear buckling terms, including hygrothermal terms, and $I_0$,$I_1$ and $I_2$ are the mass inertias which can be defined as it follows:

$$I_i = \rho \sum_{k=1}^{N_L} \int_{z_k}^{z_{k+1}} z^i \, dz \tag{14}$$

where $i = 0, 1, 2$.

## 3. Navier solution

The Navier solution is ontained for cross- and angle-ply laminates. This kind of solution allows to solve the case of simply supported plates [48].

For cross-ply laminates it is needed that $A_{16} = A_{26} = B_{16} = B_{26} = D_{16} =$

$D_{26} = 0$, and the displacement field it is assumed to be:

$$\begin{aligned} u(x,y) &= \sum_{m=1}^{\infty}\sum_{n=1}^{\infty} U_{mn} \cos\alpha x \sin\beta y \\ v(x,y) &= \sum_{m=1}^{\infty}\sum_{n=1}^{\infty} V_{mn} \sin\alpha x \cos\beta y \\ w(x,y) &= \sum_{m=1}^{\infty}\sum_{n=1}^{\infty} W_{mn} \sin\alpha x \sin\beta y \end{aligned} \tag{15}$$

For angle-ply laminates it is needed that $A_{16} = A_{26} = B_{11} = B_{12} = B_{22} = B_{66} = D_{16} = D_{26} = 0$,and the displacement field it is assumed to be:

$$\begin{aligned} u(x,y) &= \sum_{m=1}^{\infty}\sum_{n=1}^{\infty} U_{mn} \sin\alpha x \cos\beta y \\ v(x,y) &= \sum_{m=1}^{\infty}\sum_{n=1}^{\infty} V_{mn} \cos\alpha x \sin\beta y \\ w(x,y) &= \sum_{m=1}^{\infty}\sum_{n=1}^{\infty} W_{mn} \sin\alpha x \sin\beta y \end{aligned} \tag{16}$$

It is remarked the cross- and angle-ply laminated consider different kind of simply-supported boundary conditions [48].

As described in [48] shear in-plane mechanical load $\hat{N}_{xy} = 0$ should be neglected to solve the problem with Navier method. Since hygrothermal loads consider all the in-plane loads coupled, contrary to the mechanical in-plane loads, it is necessary that the lamination scheme for angle-ply plates is anti-symmetric so that it gives $\hat{N}_{xy} = 0$ (see eq. (10)). All cross-ply configurations have always $\hat{N}_{xy} = 0$.

### 3.1. Buckling

In this paragraph, the behavior of the plates subjected to thermal loads that lead to the instability will be analyzed. The solution system is:

$$\begin{bmatrix} \hat{c}_{11} & \hat{c}_{12} & \hat{c}_{13} \\ \hat{c}_{12} & \hat{c}_{22} & \hat{c}_{23} \\ \hat{c}_{13} & \hat{c}_{23} & \hat{c}_{33} + \tilde{t}_{buck} \end{bmatrix} \begin{Bmatrix} U_{mn} \\ V_{mn} \\ W_{mn} \end{Bmatrix} = \begin{Bmatrix} 0 \\ 0 \\ 0 \end{Bmatrix} \tag{17}$$

where the coefficients $\hat{c}_{ij}$ are those shown in [52] for the cross- and angle-ply plates, and the term $\tilde{t}_{buck}$ includes hygrothermal loads

$$\begin{aligned}\tilde{t}_{buck} = \bar{T}\Bigg(&\alpha^2\left(A_1^\alpha + \kappa_{c_0}A_1^\beta + \frac{\kappa_t}{h}B_1^\alpha + \frac{\kappa_{c_1}}{h}B_1^\beta\right)\\ &+ \beta^2\left(A_2^\alpha + \kappa_{c_0}A_2^\beta + \frac{\kappa_t}{h}B_2^\alpha + \frac{\kappa_{c_1}}{h}B_2^\beta\right)\Bigg)\end{aligned} \tag{18}$$

where $\kappa_{c_0} = C_0/T_0$ , $\kappa_t = T_1/T_0$ and $\kappa_{c_1} = C_1/T_0$.

From this last relation it can be deduced that the instability analysis cannot be performed with the load acting in one direction only because the type of load in question cannot be decoupled in two directions. As for the critical load, the critical temperature will be the lowest among the temperatures that lead to the instability of the plate.

$$T_{cr} = \underset{1\leq m,n\leq\infty}{\min}\left\{\bar{T}(m,n)\right\} \tag{19}$$

### *3.2. Free vibration*

Replacing the Navier displacement field in the equations of motion and neglecting the rotary inertia, in the dynamic case, we obtain the following eigenvalue problem;

$$\left(\begin{bmatrix}\hat{c}_{11} & \hat{c}_{12} & \hat{c}_{13}\\ \hat{c}_{12} & \hat{c}_{22} & \hat{c}_{23}\\ \hat{c}_{13} & \hat{c}_{23} & \hat{c}_{33}+\tilde{t}_{buck}\end{bmatrix} - \omega^2\begin{bmatrix}\hat{m}_{11} & 0 & 0\\ 0 & \hat{m}_{22} & 0\\ 0 & 0 & \hat{m}_{33}\end{bmatrix}\right)\begin{Bmatrix}U_{mn}\\ V_{mn}\\ W_{mn}\end{Bmatrix} = \begin{Bmatrix}0\\0\\0\end{Bmatrix} \tag{20}$$

where:

$$\begin{aligned}\hat{m}_{11} &= \hat{m}_{22} = I_0\\ \hat{m}_{33} &= I_0 + I_2\left(\alpha^2+\beta^2\right)\end{aligned} \tag{21}$$

For a nontrivial solution the determinant of the coefficient matrix should be zero, which yields to the characteristic polynomial. The real positive roots of this cubic equation give the square of the natural frequency associated with mode $(m, n)$. The smallest of the frequencies is called the fundamental frequency. In the present case, the applied hygrothermal pre-stress influences the stiffness of the structure, thus, natural frequencies are obtained as a function of the pre-stress. There exist a value of the applied pre-stress that leads to null natural frequencies, such temperature values are defined as critical temperatures.

## 4. Results and discussion

In this section critical temperatures for the buckling and free vibration problems are discussed. Results are compared with the existing literature to validate the present model and novel applications are reported in order to demonstrate the influence of nanoscale parameter on the buckling and free vibration modes.

### *4.1. Buckling*

The results of the first comparison are listed in table 1 with respect to the work [50], for a thin structure made of a single isotropic layer and a single orthotropic layer. For the isotropic configuration it has been considered: $E = 10^6$, $\nu = 0.3$, $\alpha_1/\alpha_0 = 1$, $\alpha_2/\alpha_0 = 1$, whereas for the orthotropic one: $E_1 = 15$, $E_2 = E_3 = 1$, $\nu_{12} = 0.3$, $\nu_{13} = 0.49$, $\nu_{23} = 0.3$, $G_{12} = 0.5$, $G_{13} = 0.3356$, $\alpha_1/\alpha_0 = 0.015$, $\alpha_2/\alpha_0 = 1$ where the normalization factor $\alpha_0 = 10^{-6}$ is taken into consideration. The results are presented in dimensionless form according to the formula $\alpha_0 T_{cr} \cdot 10^3$, where $T_{cr}$ is the critical temperature that leads the buckling into buckling mode.

| Lamina | $a/h$ | Ref. [50] | Present |
|---|---|---|---|
| Isotropic | 100 | 0.1265 | 0.1265 |
| Orthotropic | 100 | 0.7480 | 0.7486 |

Table 1: $\alpha_0 T_{cr} \cdot 10^3$ of a single square isotropic layer and a single square orthotropic layer compared with the literature $(m, n = 1)$.

Using the properties of the orthotropic layer of the first comparison laminates composed of multiple layers are analyzed. Results are shown in table 2. It is noted that the symmetric configuration (0/90/0) buckles with a non symmetric number of waves one along $x$ and two along $y$ ($m = 1$ and $n = 2$), on the contrary the antisymmetric scheme (0/90) has a symmetric buckling mode ($m = n = 1$). In both cases very good agreement is shown with the present implementation.

Another comparison has been performed with respect to the work by Shi et al [51] and comparison is listed in table 3. Mechanical properties of the plate considered are $a = 38.1$ cm, $b = 30.5$ cm, $h = 0.12$ cm, $E_1 = 155$ GPa, $E_2 = 8.07$ GPa, $G_{12} = 4.55$ GPa, $\nu_{12} = 0.22$, $\alpha_1 = -0.07 \cdot 10^{-6}$ $^\circ C^{-1}$, $\alpha_2 = 30.1 \cdot 10^{-6}$ $^\circ C^{-1}$. Very good agreement is shown considering that laboratory experiments have been carried out in [51].

| Layout | $a/h$ | Ref. [50] | Present |
|---|---|---|---|
| $(0/90)^a$ | 100 | 0.4860 | 0.4863 |
| $(0/90/0)^b$ | 100 | 0.9960 | 0.9944 |

Table 2: $\alpha_0 T_{cr} \cdot 10^3$ of a square nano-plates compared with the literature $^a(m, n = 1)$, $^b(m = 1, n = 2)$.

| Layout | $a/h$ | Ref. [51] | Present |
|---|---|---|---|
| $(0/90/90/0)_s$ | 317.5 | 6.8 °C | 6.575 °C |

Table 3: $T_{cr}$ of a cross-ply nanoplate compared with the literature $(m, n) = 1$.

#### *4.1.1. In-plane thermal load*

For the analysis of laminates with different values of the non-local parameter (tables 4, 5) the material properties are given as: $E_1/E_2 = var.$, $\nu_{12} = 0.25$, $\nu_{13} = \nu_{23} = 0$, $G_{12} = G_{13} = 0.5E_2$, $G_{23} = 0.2E_2$, $\alpha_1/\alpha_0 = 0.015$, $\alpha_2/\alpha_0 = 1$, $\beta_1 = 0$, $\beta_2 = 0.44$, where the stiffness ratio $E_1/E_2$ is variable and represents orthotropic material variation for a unitary in-plane transverse stiffness $E_2$.

Please note that the units are not reported because a consistent system has been implicitly considered. moreover, with the present selection the results are dimensionless for the thermal case only. Whereas, the results will be reported in factorized form for the hygrothermal applications. The plates considered are rectangular with a ratio $a/h = 100$ and the total height of the laminate is kept constant independently on the number of plies in each stack.

From tables 4, 5 it can be noticed that the critical temperature is higher for angle-ply laminates than for cross-ply ones with the same number of laminae. For antisymmetric cross- and angle-ply plates the instability always occurs for $(m, n) = (1, 1)$, whereas for symmetrical cross-ply plates the instability comes for different values of $(m, n)$. In addition when the nonlocal parameter increases the critical temperature also increases.

Figure 2 displays different behaviours of cross- and angle-ply laminates by varying the geometric $a/b$ and stiffness $E_1/E_2$ ratios for different values of the nonlocal parameter. It must be underlined that is considered $a = 1$ for the variation $a/b$, since such results are not reported in dimentionless form but they are factorized by $\alpha_0 T_{cr}$. The critical buckling temperatures increase almost exponentially by enlarging the plate width in the direction transverse

| $(\ell/a)^2$ | $a/b$ | $E_1/E_2$ | | | | |
|---|---|---|---|---|---|---|
| | | 5 | 10 | 20 | 25 | 40 |
| | | | | (0/90/0) | | |
| 0.00 | 0.5 | $0.5246^{(1,2)}$ | $0.7522^{(1,3)}$ | $1.0529^{(1,3)}$ | $1.1855^{(1,3)}$ | $1.5277^{(1,3)}$ |
| | 1.0 | 0.5246 | 0.7902 | $1.1309^{(1,2)}$ | $1.2413^{(1,2)}$ | $1.5302^{(1,2)}$ |
| | 1.5 | 0.5803 | 0.7522 | 1.0529 | 1.1855 | 1.5277 |
| 0.05 | 0.5 | 0.9885 | $1.5702^{(1,2)}$ | $2.4710^{(1,2)}$ | $2.8591^{(1,2)}$ | $3.8346^{(1,2)}$ |
| | 1.0 | 1.0423 | 1.5702 | 2.4710 | 3.4050 | 3.8346 |
| | 1.5 | 1.5111 | 1.9587 | 2.7415 | 2.8591 | 3.9779 |
| 0.10 | 0.5 | 1.3656 | $2.3501^{(1,2)}$ | $3.6984^{(1,2)}$ | $4.2792^{(1,2)}$ | $5.7392^{(1,2)}$ |
| | 1.0 | 1.5601 | 2.3501 | 3.6984 | 4.2792 | 5.7392 |
| | 1.5 | 2.4418 | 3.1651 | 4.4301 | 4.9882 | 6.4280 |
| | | | | $(0/90)_2$ | | |
| 0.00 | 0.5 | 0.3494 | 0.5357 | 0.8510 | 0.9864 | 1.3267 |
| | 1.0 | 0.4908 | 0.7549 | 1.0688 | 1.2250 | 1.6174 |
| | 1.5 | 0.8432 | 1.2477 | 1.9323 | 2.2265 | 2.9657 |
| 0.05 | 0.5 | 0.5651 | 0.8663 | 1.3759 | 1.5949 | 2.1450 |
| | 1.0 | 0.9752 | 1.4018 | 2.1238 | 2.4341 | 3.2137 |
| | 1.5 | 2.1956 | 3.2489 | 5.0314 | 5.7975 | 7.7221 |
| 0.10 | 0.5 | 0.7807 | 1.1968 | 1.9008 | 2.2033 | 2.9634 |
| | 1.0 | 1.4597 | 2.0981 | 3.1787 | 3.6432 | 4.8101 |
| | 1.5 | 3.5480 | 5.2501 | 8.1304 | 9.3684 | 12.4785 |

Table 4: $\alpha_0 T_{cr} \cdot 10^3$ of different cross-ply laminates for different values of the geometric $a/b$ and stiffness $E_1/E_2$ and the non-local parameter $(\ell/a)^2$. The superscripts indicate the number of semi-waves for which the plate becomes unstable $^{(m,n)}$, where $(m,n) = (1,1)$ is not indicated.

| $(\ell/a)^2$ | $a/b$ | 5 | 10 | 20 | 25 | 40 |
|---|---|---|---|---|---|---|
| | | | | $E_1/E_2$ | | |
| | | | | $(-45/45)$ | | |
| 0.00 | 0.5 | 0.2855 | 0.3580 | 0.4656 | 0.5102 | 0.6206 |
| | 1.0 | 0.4951 | 0.6418 | 0.8583 | 0.9478 | 1.1693 |
| | 1.5 | 0.7790 | 0.9967 | 1.3189 | 1.4521 | 1.7822 |
| 0.05 | 0.5 | 0.4617 | 0.5789 | 0.7528 | 0.8249 | 1.0034 |
| | 1.0 | 0.9839 | 1.2753 | 1.7054 | 1.8832 | 2.3232 |
| | 1.5 | 2.0283 | 2.5952 | 3.4340 | 3.7811 | 4.6404 |
| 0.10 | 0.5 | 0.6378 | 0.7997 | 1.0401 | 1.1397 | 1.3862 |
| | 1.0 | 1.4726 | 1.9088 | 2.5525 | 2.8186 | 3.4773 |
| | 1.5 | 3.2776 | 4.1938 | 5.5549 | 6.1102 | 7.4987 |
| | | | | $(-45/45)_2$ | | |
| 0.00 | 0.5 | 0.3827 | 0.6096 | 0.9932 | 1.1581 | 1.5723 |
| | 1.0 | 0.6809 | 1.1271 | 1.8820 | 2.2063 | 3.0209 |
| | 1.5 | 1.0607 | 1.7302 | 2.8627 | 3.3493 | 4.5716 |
| 0.05 | 0.5 | 0.6188 | 0.9856 | 1.6059 | 1.8725 | 2.5421 |
| | 1.0 | 1.3529 | 2.2397 | 3.7395 | 4.3839 | 6.0025 |
| | 1.5 | 2.7617 | 4.5052 | 7.4539 | 8.7209 | 11.9035 |
| 0.10 | 0.5 | 0.8549 | 1.3616 | 2.2186 | 2.5869 | 3.5120 |
| | 1.0 | 2.0249 | 3.3522 | 5.5969 | 6.5614 | 8.9840 |
| | 1.5 | 4.4629 | 7.2801 | 12.0450 | 14.0925 | 19.2354 |

Table 5: $\alpha_0 T_{cr} \cdot 10^3$ of different angle-ply laminates for different values of the geometric $a/b$ and stiffness $E_1/E_2$ and the non-local parameter $(\ell/a)^2$. $(m, n) = (1, 1)$.

| $(\ell/a)^2$ | $\kappa_t$ | $E_1/E_2$ | | | | |
|---|---|---|---|---|---|---|
| | | 5 | 10 | 20 | 25 | 40 |
| 0.00 | 0 | 0.8432 | 1.2477 | 1.9323 | 2.2265 | 2.9657 |
| | 5 | 0.9613 | 1.3916 | 2.0782 | 2.3584 | 3.0260 |
| | 10 | 1.1177 | 1.5730 | 2.2479 | 2.5068 | 3.0889 |
| 0.05 | 0 | 2.1956 | 3.2489 | 5.0314 | 5.7975 | 7.7221 |
| | 5 | 2.5029 | 3.6235 | 5.4112 | 6.1408 | 7.8792 |
| | 10 | 2.9103 | 4.0958 | 5.8532 | 6.5272 | 8.0428 |
| 0.10 | 0 | 3.5840 | 5.2501 | 8.1304 | 9.3684 | 12.4785 |
| | 5 | 4.0446 | 5.8554 | 8.7443 | 9.9231 | 12.7324 |
| | 10 | 4.7029 | 6.6186 | 9.4584 | 10.5477 | 12.9968 |

Table 6: $\alpha_0 T_{0,cr} \cdot 10^3$ of a rectangular plate ($a/b = 1.5$) with lamination layout $(0/90)_2$ for different value of ratio $\kappa_t = T_{1,cr}/T_{0,cr}$ and non local parameter $(\ell/a)^2$.$(m, n) = (1, 1)$.

to the fibers (zero fiber angle corresponds to the $x$ axis which is related to plate width $a$).

*4.1.2. In-plane and bending thermal loads*

The effect of constant and linear thermal loads is investigated below. The aim is to show the effect of a linear temperature field to the buckling of the plate, this effect is considered with the coefficient $\kappa_t = T_{1,cr}/T_{0,cr}$. Table 6 shows the buckling when combined thermal load for cross-ply laminates is considered. The plate is of rectangular shape $a/b = 1.5$ with $a = 1$ and anti-symmetric cross-ply configuration. It is clear that the buckling temperature increases as the linear temperature increases, this induces the plate to show a stiffer behavior. Such increase is observed by increasing the stiffness ratio $E_1/E_2$ and the nonlocal parameter. Figure 3 shows the different behavior of nanoplates when they are subjected to a uniform and linear combination of temperature along the thickness for different geometric ratios $a/b$ with $a = 1$. It should be remarked that the effect of combining constant and linear temperature distributions does not effect the critical temperature for square plates since all the curves coincide for $a/b = 1$. Overall small effects on the critical temperature are observed by including a linear temperature distribution.

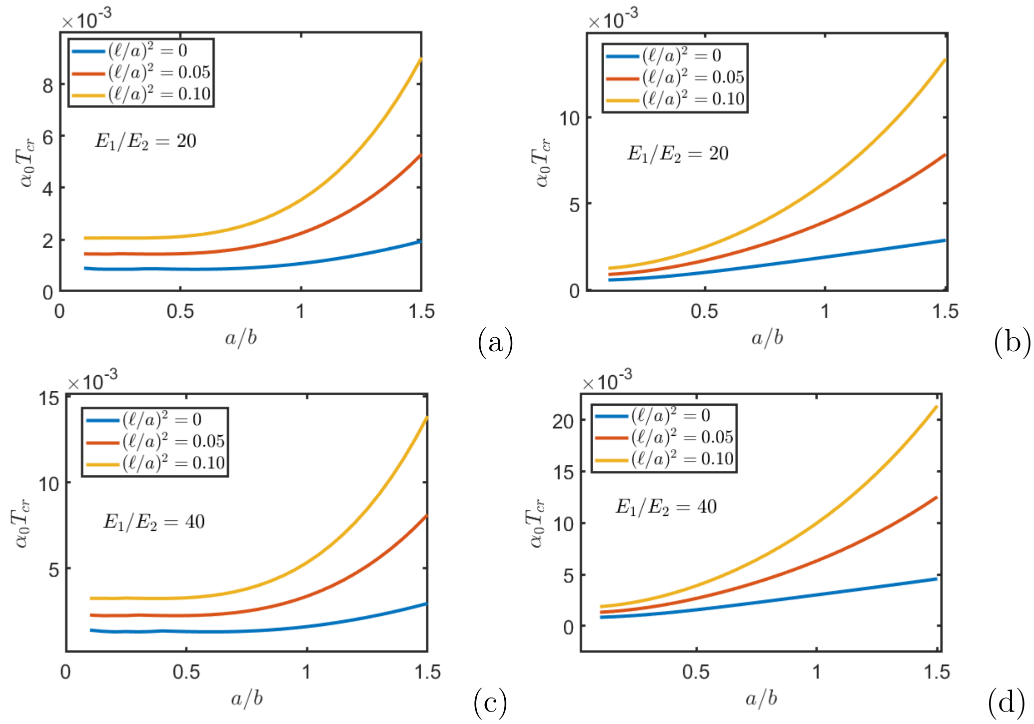


Figure 2: Critical temperature ($\alpha_0 T_{cr}$) of plates $(0/90)_2$ (a,c) and $(-45/45)_2$ (b,d) for different $a/b$ and different value of non local parameter $(\ell/a)^2$.

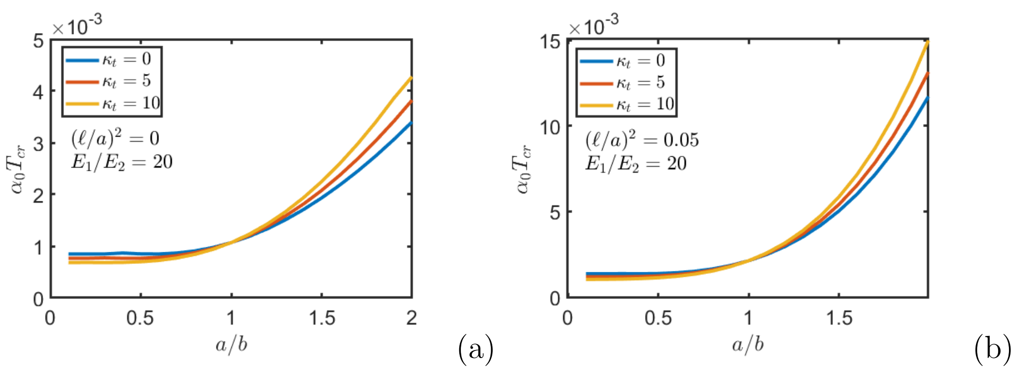


Figure 3: Critical temperature $\alpha_0 T_{cr}$ of plate with lamination layout $(0/90)_2$ for $(\ell/a)^2 = 0$ (a) and for $(\ell/a)^2 = 0.05$ (b) to vary of $\kappa_t$.

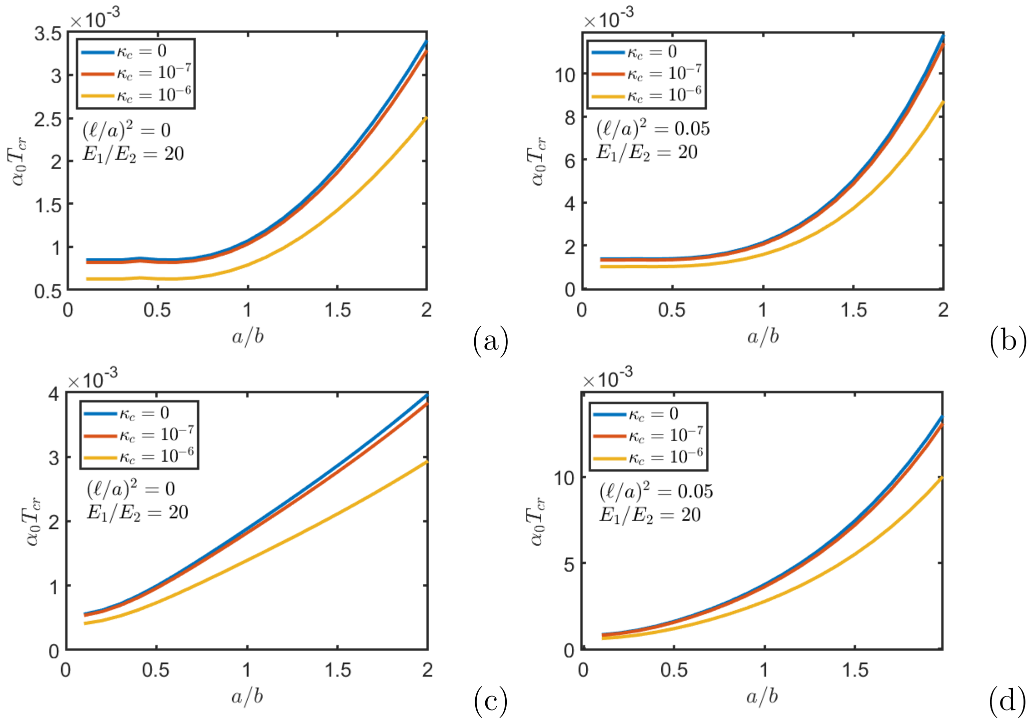


Figure 4: Critical temperature $\alpha_0 T_{cr}$ of plate by varying $\kappa_{c_0}$ with lamination layout $(0/90)_2$ for $(\ell/a)^2 = 0$ (a) and for $(\ell/a)^2 = 0.05$ (b) with lamination layout $(-45/45)_2$ for $(\ell/a)^2 = 0$ (c) and for $(\ell/a)^2 = 0.05$ (d).

#### *4.1.3. Hygrothermal loads*

For hygrothermal a rectangular plate with ratio $a/b = 1.5$ with $a = 1$ is considered. Table 7 lists the combined buckling loads with $\kappa_{c_0} = C_{0,cr}/T_{0,cr}$ for both cross- and angle-ply laminates. Globally the critical temperature increases, as in the previous cases, by increasing the stiffness ratio $E_1/E_2$ and the nonlocal parameter. It is mentioned that by increasing the ratio $\kappa_{c_0} = C_{0,cr}/T_{0,cr}$, the critical temperature decreases because the critical load is weighted between the two values of $C_{0,cr}$ and $T_{0,cr}$. Figure 4 show the critical temperature for cross- and angle-play laminates, when they are subjected to hygrothermal load combination. It is noted that the angle-ply laminates have a smaller exponential increase with respect to the cross-ply ones by varying the geometric ratio $a/b$ for $a = 1$.

| $(\ell/a)^2$ | $\kappa_{c_0}$ | $E_1/E_2$ 5 | 10 | 20 | 25 | 40 |
|---|---|---|---|---|---|---|
| | | $(0/90)_2$ | | | | |
| 0.00 | 0 | 0.8432 | 1.2477 | 1.9323 | 2.2265 | 2.9657 |
| | $10^{-7}$ | 0.8097 | 1.2007 | 1.8662 | 2.1538 | 2.8802 |
| | $10^{-6}$ | 0.5964 | 0.8965 | 1.4271 | 1.6645 | 2.2871 |
| 0.05 | 0 | 2.1956 | 3.2489 | 5.0314 | 5.7975 | 7.7221 |
| | $10^{-7}$ | 2.1083 | 3.1264 | 4.8594 | 5.6081 | 7.4996 |
| | $10^{-6}$ | 1.5528 | 2.3343 | 3.7160 | 4.3340 | 5.9552 |
| 0.10 | 0 | 3.5840 | 5.2501 | 8.1304 | 9.3684 | 12.4785 |
| | $10^{-7}$ | 3.4069 | 5.0521 | 7.8525 | 9.0624 | 12.1189 |
| | $10^{-6}$ | 2.5093 | 3.7721 | 6.0048 | 7.0035 | 9.6233 |
| | | $(-45/45)_2$ | | | | |
| 0.00 | 0 | 1.0607 | 1.7302 | 2.8627 | 3.3493 | 4.5716 |
| | $10^{-7}$ | 1.0185 | 1.6650 | 2.1143 | 3.2399 | 4.4398 |
| | $10^{-6}$ | 0.7502 | 1.2431 | 2.2479 | 2.5038 | 3.5255 |
| 0.05 | 0 | 2.7618 | 4.5052 | 7.4539 | 8.7209 | 11.9035 |
| | $10^{-7}$ | 2.6520 | 4.3353 | 7.1990 | 8.4360 | 11.5605 |
| | $10^{-6}$ | 1.9533 | 3.2369 | 5.5051 | 6.5194 | 9.1798 |
| 0.10 | 0 | 4.4629 | 7.2801 | 12.0451 | 14.0925 | 19.2354 |
| | $10^{-7}$ | 4.2855 | 7.0056 | 11.6333 | 13.6322 | 18.6811 |
| | $10^{-6}$ | 3.1564 | 5.2307 | 8.8960 | 10.5350 | 14.8341 |

Table 7: $\alpha_0 T_{0,cr} \cdot 10^3$ of a rectangular plate ($a/b = 1.5$) with lamination layout $(0/90)_2$ for different value of ratio $\kappa_{c_0} = C_{0,cr}/T_{0,cr}$ and non local parameter $(\ell/a)^2$. $(m,n) = (1,1)$.

*4.2. Free Vibration*

In this section results of free vibration, including thermal effects, are reported. The critical temperature will be analyzed, which corresponds to the temperature at which the natural frequency of free vibration becomes zero. The following material properties are used in the computations below: $E_1/E_2 = var.$, $\nu_{12} = 0.25$, $\nu_{13} = \nu_{23} = 0$, $G_{12} = G_{13} = 0.5E_2$, $G_{23} = 0.2E_2$, $\alpha_1/\alpha_0 = 1$, $\alpha_2/\alpha_0 = 3$. The plate is considered squared $a = b = 1$ for all numerical simulations. Natural frequencies are factorized as:

- cross-ply: $\bar{\omega} = \omega b^2/\pi^2\sqrt{\rho h/D_{22}}$
- angle-ply: $\bar{\omega} = \omega a^2/h\sqrt{\rho/E_2}$

Table 8 lists the results compared to [48, 52]. The results of the present work agree well with the ones presented in former literature but these results do not include any hygrothermal effect.

Figure 5 shows the influence of temperature in natural vibration frequencies of cross- and angle-ply laminates for different values of non local parameter and different lamination layouts. By reducing the temperature a detrimental effect is observed in the structural stiffness since the main natural frequency reduces garishly. There exists a temperature value for which the natural frequency is equal to zero, that temperature is called critical temperature for free vibrations. It can be noted that critical temperature for angle-ply laminates is higher than those of cross-ply laminates for plates with same number of laminae. In other words angle-ply laminates are able to vibrate at higher temperatures with respect to cross-ply before collapse. The same evidence in reported in tabular form in table 9 where critical temperatures for cross- and angle-ply laminates are provided.

## 5. Conclusions

In this paper, hygrothermal buckling and dynamic problems of simply supported composite nano plates were investigated. Non local second strain gradient theory is implemented for taking into account the effects of nano scale. Through Hamilton's principle motion equations for laminated composite thin plates are derived. The analytical solution using Navier solution method is obtained. Several plate layouts, materials and geometries are involved, comparisons for the classical case wherever it was possible are provided, then outcomes are extended to non local theory. Firstly outcomes for

| Layout | $(\ell/a)^2$ | Ref. [48] | Ref. [52] | Present |
|---|---|---|---|---|
| | | $E_1/E_2 = 10$ | | |
| (0/90) | 0 | 1.183 | 1.183 | 1.183 |
| | 0.05 | — | 1.668 | 1.668 |
| | 0.10 | — | 2.041 | 2.040 |
| $(0/90)_4$ | 0 | 1.545 | 1.545 | 1.545 |
| | 0.05 | — | 2.178 | 2.177 |
| | 0.10 | — | 2.664 | 2.664 |
| | | $E_1/E_2 = 20$ | | |
| (0/90) | 0 | 0.990 | 0.990 | 0.990 |
| | 0.05 | — | 1.395 | 1.395 |
| | 0.10 | — | 1.707 | 1.707 |
| $(0/90)_4$ | 0 | 1.469 | 1.469 | 1.469 |
| | 0.05 | — | 2.071 | 2.071 |
| | 0.10 | — | 2.534 | 2.534 |
| | | $E_1/E_2 = 25$ | | |
| $(-45/45)$ | 0 | 12.357 | 12.358 | 12.357 |
| | 0.05 | — | 17.419 | 17.419 |
| | 0.10 | — | 21.311 | 21.310 |
| $(-45/45)_4$ | 0 | 20.154 | 20.154 | 20.154 |
| | 0.05 | — | 28.409 | 28.409 |
| | 0.10 | — | 34.756 | 34.756 |
| | | $E_1/E_2 = 40$ | | |
| $(-45/45)$ | 0 | 14.636 | 14.636 | 14.636 |
| | 0.05 | — | 20.631 | 20.630 |
| | 0.10 | — | 25.241 | 25.239 |
| $(-45/45)_3$ | 0 | 24.825 | 24.825 | 24.825 |
| | 0.05 | — | 34.994 | 34.994 |
| | 0.10 | — | 42.812 | 42.811 |

Table 8: Fundamental frequencies $\bar{\omega}$ for cross- and angle-ply laminates.

| $(\ell/a)^2$ | (0/90) | $(0/90)_4$ | $(-45/45)$ | $(-45/45)_4$ |
|---|---|---|---|---|
| 0 | 35.2506 | 77.6826 | 55.5655 | 138.4088 |
| 0.05 | 70.0422 | 154.3526 | 110.4064 | 275.0129 |
| 0.10 | 104.8334 | 231.0231 | 165.2473 | 411.6170 |

Table 9: Critical temperature $T_{0,cr}$ for cross- and angle-ply laminates with $E_1/E_2 = 20$.

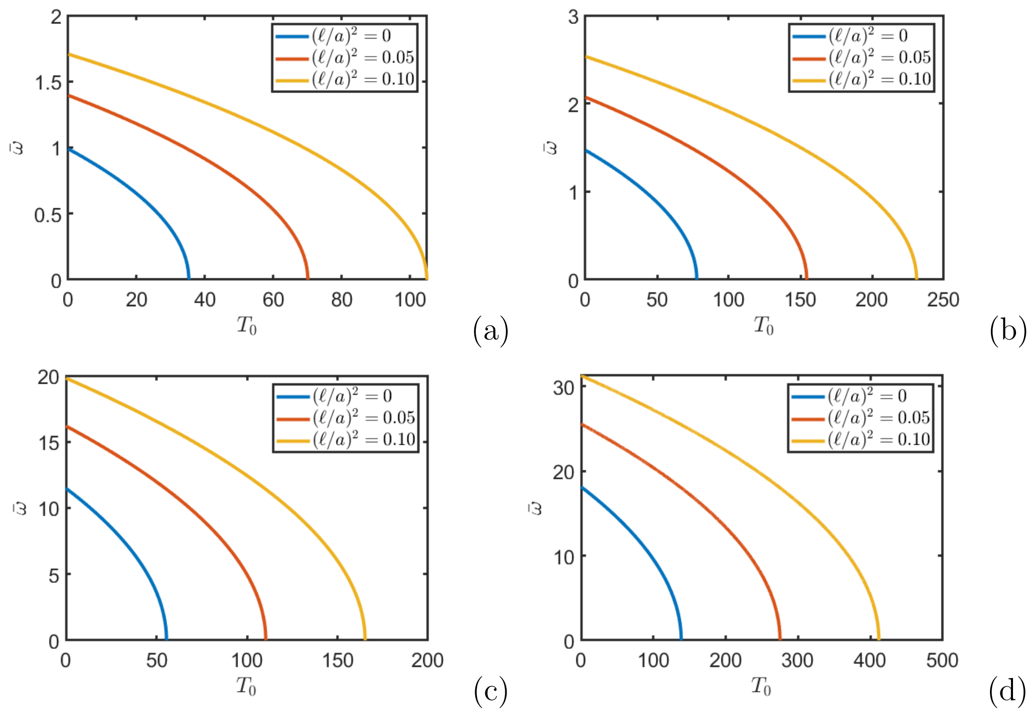


Figure 5: Natural frequency ($\bar{\omega}$) versus temperature ($T_0$) with $E_1/E_2 = 20$ for (a) (0/90) , (b) $(0/90)_4$ , (c) $(-45/45)$ and (d) $(-45/45)_4$.

thermal and combined hygrothermal buckling of cross- and angle-ply laminates are provided, it can be seen that for the same number of laminae, angle-ply laminates are preferable, moreover for the same thickness is better to have more laminae. Finally outcomes for free vibration are reported. At first the classic problem is investigated and compared, then thermal terms are included and the critical temperatures for various lamination layouts and values of non local parameter is obtained. Also in this case, angle-ply laminates show a better behavior than cross-ply ones.

## References


[1] V. S. Saji, H. C. Choe, K. W. Yeung, Nanotechnology in biomedical applications: a review, International Journal of Nano and Biomaterials 3 (2010) 119–139.

[2] D. Berman, J. Krim, Surface science, MEMS and NEMS: Progress and opportunities for surface science research performed on, or by, microdevices, Progress in Surface Science 88 (2013) 171 – 211.

[3] B. Bhushan, Nanotribology and nanomechanics of MEMS/NEMS and bioMEMS/bioNEMS materials and devices, Microelectronic Engineering 84 (2007) 387 – 412. Nanoscale imaging and metrology of devices and innovative materials.

[4] K. L. Ekinci, M. L. Roukes, Nanoelectromechanical systems, Review of Scientific Instruments 76 (2005) 061101.

[5] A. Bonanni, M. del Valle, Use of nanomaterials for impedimetric DNA sensors: A review, Analytica Chimica Acta 678 (2010) 7 – 17.

[6] W. Wu, Inorganic nanomaterials for printed electronics: a review, Nanoscale 9 (2017) 7342–7372.

[7] O. Gohardani, M. C. Elola, C. Elizetxea, Potential and prospective implementation of carbon nanotubes on next generation aircraft and space vehicles: A review of current and expected applications in aerospace sciences, Progress in Aerospace Sciences 70 (2014) 42 – 68.

[8] T. Singh, A review of nanomaterials in civil engineering works, Inter J Struct Civ Eng Res 3 (2014) 31–5.

[9] A. W. McFarland, J. S. Colton, Role of material microstructure in plate stiffness with relevance to microcantilever sensors, Journal of Micromechanics and Microengineering 15 (2005) 1060–1067.

[10] D. Lam, F. Yang, A. Chong, J. Wang, P. Tong, Experiments and theory in strain gradient elasticity, Journal of the Mechanics and Physics of Solids 51 (2003) 1477 – 1508.

[11] R. Lakes, Experimental microelasticity of two porous solids, International Journal of Solids and Structures 22 (1986) 55 – 63.

[12] J. Stölken, A. Evans, A microbend test method for measuring the plasticity length scale, Acta Materialia 46 (1998) 5109 – 5115.

[13] A. Eringen, D. Edelen, On nonlocal elasticity, International Journal of Engineering Science 10 (1972) 233 – 248.

[14] P. Trovalusci, Molecular Approaches for Multifield Continua: origins and current developments, 2014, pp. 211–278.

[15] A. C. Eringen, On differential equations of nonlocal elasticity and solutions of screw dislocation and surface waves, Journal of Applied Physics 54 (1983) 4703–4710.

[16] E. Aifantis, Update on a class of gradient theories, Mechanics of Materials 35 (2003) 259 – 280.

[17] J. Meenen, H. Altenbach, V. Eremeyev, K. Naumenko, A variationally consistent derivation of microcontinuum theories, Advanced Structured Materials 15 (2011).

[18] R. Mindlin, N. Eshel, On first strain-gradient theories in linear elasticity, International Journal of Solids and Structures 4 (1968) 109 – 124.

[19] B. Karami, M. Janghorban, T. Rabczuk, Static analysis of functionally graded anisotropic nanoplates using nonlocal strain gradient theory, Composite Structures 227 (2019) 111249.

[20] V. Eremeyev, H. Altenbach, On the Direct Approach in the Theory of Second Gradient Plates, volume 45, 2015, pp. 147–154.

[21] M. Bacciocchi, N. Fantuzzi, A. Ferreira, Conforming and nonconforming laminated finite element Kirchhoff nanoplates in bending using strain gradient theory, Computers & Structures 239 (2020) 106322.

[22] R. Barretta, L. Feo, R. Luciano, F. Marotti de Sciarra, R. Penna, Functionally graded Timoshenko nanobeams: A novel nonlocal gradient formulation, Composites Part B: Engineering 100 (2016) 208 – 219.

[23] S. Sahmani, M. M. Aghdam, T. Rabczuk, Nonlinear bending of functionally graded porous micro/nano-beams reinforced with graphene platelets based upon nonlocal strain gradient theory, Composite Structures 186 (2018) 68 – 78.

[24] A. Jamalpoor, M. Hosseini, Biaxial buckling analysis of double-orthotropic microplate-systems including in-plane magnetic field based on strain gradient theory, Composites Part B: Engineering 75 (2015) 53 – 64.

[25] A. Apuzzo, R. Barretta, S. Faghidian, R. Luciano, F. Marotti de Sciarra, Free vibrations of elastic beams by modified nonlocal strain gradient theory, International Journal of Engineering Science 133 (2018) 99 – 108.

[26] F. Yang, A. Chong, D. Lam, P. Tong, Couple stress based strain gradient theory for elasticity, International Journal of Solids and Structures 39 (2002) 2731 – 2743.

[27] H. Mühlhaus, F. Oka, Dispersion and wave propagation in discrete and continuous models for granular materials, International Journal of Solids and Structures 33 (1996) 2841 – 2858.

[28] L. Leonetti, F. Greco, P. Trovalusci, R. Luciano, R. Masiani, A multiscale damage analysis of periodic composites using a couple-stress/Cauchy multidomain model: Application to masonry structures, Composites Part B: Engineering 141 (2018) 50 – 59.

[29] A. Farajpour, C. Q. Howard, W. S. Robertson, On size-dependent mechanics of nanoplates, International Journal of Engineering Science 156 (2020) 103368.

[30] R. Barretta, S. A. Faghidian, F. Marotti de Sciarra, Stress-driven nonlocal integral elasticity for axisymmetric nano-plates, International Journal of Engineering Science 136 (2019) 38 – 52.

[31] P. Trovalusci, M. D. Bellis, M. Ostoja-Starzewski, A statistically-based homogenization approach for particle random composites as micropolar continua., Advanced Structured Materials 42 (2016).

[32] E. Reccia, M. L. De Bellis, P. Trovalusci, R. Masiani, Sensitivity to material contrast in homogenization of random particle composites as micropolar continua, Composites Part B: Engineering 136 (2018) 39 – 45.

[33] N. Fantuzzi, L. Leonetti, P. Trovalusci, F. Tornabene, Some novel numerical applications of Cosserat continua, International Journal of Computational Methods 15 (2018) 1850054.

[34] F. Pinnola, S. A. Faghidian, R. Barretta, F. Marotti de Sciarra, Variationally consistent dynamics of nonlocal gradient elastic beams, International Journal of Engineering Science 149 (2020) 103220.

[35] M. Mohammadimehr, M. Salemi, B. Rousta Navi, Bending, buckling, and free vibration analysis of MSGT microcomposite Reddy plate reinforced by FG-SWCNTs with temperature-dependent material properties under hydro-thermo-mechanical loadings using DQM, Composite Structures 138 (2016) 361 – 380.

[36] M. Arefi, A. M. Zenkour, Thermo-electro-mechanical bending behavior of sandwich nanoplate integrated with piezoelectric face-sheets based on trigonometric plate theory, Composite Structures 162 (2017) 108 – 122.

[37] J. Yan, L. Tong, C. Li, Y. Zhu, Z. Wang, Exact solutions of bending deflections for nano-beams and nano-plates based on nonlocal elasticity theory, Composite Structures 125 (2015) 304 – 313.

[38] C. H. Thai, A. Ferreira, P. Phung-Van, A nonlocal strain gradient isogeometric model for free vibration and bending analyses of functionally graded plates, Composite Structures 251 (2020) 112634.

[39] L. Lu, X. Guo, J. Zhao, Size-dependent vibration analysis of nanobeams based on the nonlocal strain gradient theory, International Journal of Engineering Science 116 (2017) 12 – 24.

[40] H. Daghigh, V. Daghigh, A. Milani, D. Tannant, T. E. Lacy, J. Reddy, Nonlocal bending and buckling of agglomerated cnt-reinforced composite nanoplates, Composites Part B: Engineering 183 (2020) 107716.

[41] A. Jafari, S. Shirvani Shah-enayati, A. A. Atai, Size dependency in vibration analysis of nano plates; one problem, different answers, European Journal of Mechanics - A/Solids 59 (2016) 124 – 139.

[42] O. Civalek, C. Demir, B. Akgoz, Free vibration and bending analyses of cantilever microtubules based on nonlocal continuum model, Mathematical and Computational Applications 15 (2010) 289 – 298.

[43] L. Chu, G. Dui, Y. Zheng, Thermally induced nonlinear dynamic analysis of temperature-dependent functionally graded flexoelectric nanobeams based on nonlocal simplified strain gradient elasticity theory, European Journal of Mechanics - A/Solids 82 (2020) 103999.

[44] S. Brischetto, R. Leetsch, E. Carrera, T. Wallmersperger, B. Kröplin, Thermo-mechanical bending of functionally graded plates, Journal of Thermal Stresses 31 (2008) 286–308.

[45] S. Brischetto, Hygrothermal loading effects in bending analysis of multilayered composite plates, Computer Modeling in Engineering & Sciences 88 (2012) 367–418.

[46] S. Brischetto, E. Carrera, Coupled thermo-electro-mechanical analysis of smart plates embedding composite and piezoelectric layers, Journal of Thermal Stresses 35 (2012) 766–804.

[47] S. Brischetto, E. Carrera, Static analysis of multilayered smart shells subjected to mechanical, thermal and electrical loads, Meccanica 48 (2013) 1263–1287.

[48] J. Reddy, Mechanics of Laminated Composite Plates and Shells: Theory and Analysis, Second Edition, CRC Press, 2003.

[49] F. Cornacchia, N. Fantuzzi, R. Luciano, R. Penna, Solution for cross- and angle-ply laminated Kirchhoff nano plates in bending using strain gradient theory, Composites Part B: Engineering 173 (2019) 107006.

[50] H. Matsunaga, Thermal buckling of cross-ply laminated composite and sandwich plates according to a global higher-order deformation theory, Composite Structures 68 (2005) 439 – 454.

[51] C. M. Yucheng Shi, Raymond Y. Y. Lee, Thermal postbuckling of composite plates using the finite element model coordinate method, Journal of Thermal Stresses 22 (1999) 595–614.

[52] F. Cornacchia, F. Fabbrocino, N. Fantuzzi, R. Luciano, R. Penna, Analytical solution of cross- and angle-ply nano plates with strain gradient theory for linear vibrations and buckling, Mechanics of Advanced Materials and Structures (2019).